CFD based simulation of Longitudinal Flight Mechanics with Control

M.R.Allan*, K.J.Badcock†and B.E.Richards‡
Computational Fluid Dynamics Laboratory,
Department of Aerospace Engineering,
University of Glasgow, G12 8QQ,
United Kingdom.

Computational Fluid Dynamics based simulation of trimmed flight is now becoming possible but requires the incorporation of a controller which commands control surface deflections. This paper describes efforts to realise this for a generic fighter configuration in longitudinal motions. The incorporation of the flight mechanics equations and controller into the CFD solver loop and the treatment of the mesh, which must move with both the control surface deformations and the rigid motion of the aircraft, are described. This work is a contribution to a wider effort towards the simulation of aeroelastic and flight stability in regions where nonlinear aerodynamics, and hence potentially CFD, can play a key role. Results demonstrating the coupled solution are presented.

I. Introduction

The basis of conventional flight mechanics models is a coefficient based description of the aerodynamics, with the coefficients (stability derivatives) being obtained from experiment. The control inputs enter the model as aerodynamic data from tables.

The flight simulation therefore depends to a large extent on the quality of the aerodynamic model. There is potential for some rather complex aerodynamic phenomena which incorporate significant hysteresis which will not be described by derivative based aerodynamic models (see for example[1]). In principle computational fluid dynamics can produce the aerodynamic inputs but can also, through a coupling with rigid body motion equations, simulate a rigid motion response directly. Although not likely to be a tool for routine flight mechanics studies, such a simulation could be very powerful for investigating and understanding potential problem conditions. In addition aeroelastic stability studies of flexible aircraft based on CFD should incorporate the influence of the flight control system.

The current paper describes work to put in place a CFD based simulation of flight mechanics. The intention here is not to investigate complex flight mechanics behaviour, but to describe the development of a tool which can be used for this purpose. Issues addressed are the coupling of the CFD and the flight mechanics models, incorporation of flight control for longitudinally unstable configurations and grid treatment for moving control surfaces on a rigidly moving aircraft.

II. Flow solver

All simulations described were performed using the University of Glasgow PMB (Parallel Multi-Block) RANS solver. A full discussion of the code and turbulence models implemented is given in reference.[2] PMB uses a cell centred finite volume technique to solve the Euler and RANS equations. The diffusive terms

*Research Assistant
†Reader
‡Emeritus Professor

Copyright © M.R.Allan, K.J.Badcock and B.E.Richards by. Published by the American Institute of Aeronautics and Astronautics, Inc. with permission.ff

are discretised using a central differencing scheme, and the convective terms using Osher's approximate Riemann solver with MUSCL interpolation. Steady flow calculations proceed in two parts, initially running an explicit scheme, then switching to an implicit scheme to obtain faster convergence. The linear system arising at each implicit step is solved using a Krylov subspace method. The preconditioning is based on a Block Incomplete Lower-Upper BILU(0) factorisation which is decoupled across blocks. For time-accurate simulations, Jameson's pseudo-time (dual-time stepping) formulation is applied,[3] with the steady state solver used to calculate the flow steady states on each physical time step.

III. Longitudinal Flight Mechanics Models

Two flight mechanics models have been implemented, a 1 degree-of-freedom free-to-pitch model about the body pitch axis, and a 3 degree-of-freedom free-to-pitch model and translate in the longitudinal plane.

A. Free-to-pitch model

The non-dimensional one degree-of-freedom pitch model is given by

$$\frac{\ddot{\theta}^* {c_r^*}^2}{U_\infty^{*2}} = \ddot{\theta} = \frac{\rho_\infty^* {c_r^*}^5}{J_{zz}^*} C_{M_z} \tag{1}$$

where $\ddot{\theta}$ is the non-dimensional pitch acceleration, ρ_∞^* is the freestream air density, c_r^* is the root chord of the wing, J_{zz}^* is the moment of inertia around the body z-axis, and C_{M_z} is the pitching moment around the body z-axis. In the coordinate system employed by the PMB flow solver, J_{zz} is the moment of inertia about the pitch axis which points spanwards in the body fixed coordinate system.

In the current work the pitching moment coefficient is defined as

$$C_m = \frac{C_{M_z}}{\rho_\infty U_\infty^2 c_r^3} \tag{2}$$

The one degree-of-freedom model was coupled to the PMB solver by evaluating the flight mechanics model in the pseudo time stepping loop of the dual time stepping scheme of Jameson.[3] In this way, the flight mechanics model converges with the flow solution minimising sequencing errors. Clearly the only variable driving the pitching motion is the pitching moment coefficient which is updated at each pseudo time step. The most recent update for the pitching moment C_m is used in the evaluation of the pitch angle and pitch rate at the following pseudo time step.

The implicit integration scheme is given by

$$\mathbf{q}^{n+1,k} = \mathbf{q}^n + \frac{\Delta\tau}{2}(\mathbf{R}^{n+1,k} + \mathbf{R}^n) \tag{3}$$

where

$$\mathbf{q} = (\theta_\tau, \theta)^T \tag{4}$$

and

$$\mathbf{R} = (\frac{\rho_\infty c_r^5}{J_{zz}} C_m, \theta_\tau)^T. \tag{5}$$

Note that for 1 DOF pitching motion $\theta = \alpha$. With the updated position of the wing θ, the grid is rigidly rotated and the grid speeds are computed with second order finite differences.

B. Longitudinal 3 degree of Freedom Model

The dimensional translational equations of motion (for a flat Earth inertial reference frame) is

$$\dot{\mathbf{U}}_B^* = \frac{1}{M^*}{\mathbf{F}^*}_B - \omega_B^* \times \mathbf{U}_B^* + \mathbf{B}\mathbf{g}_I^* \tag{6}$$

where

$$\dot{\mathbf{U}}_B = (\dot{u}_B, \dot{v}_B, 0)^T \tag{7}$$

$$\mathbf{F}_B = (F_x + T, F_y, 0)^T \tag{8}$$

$$\omega_B = \left(0, 0, \dot{\theta}\right)^T \tag{9}$$

$$\mathbf{B} = \begin{bmatrix} cos\theta & sin\theta & 0 \\ -sin\theta & cos\theta & 0 \\ 0 & 0 & 1 \end{bmatrix} \tag{10}$$

$$\tag{11}$$

and $\mathbf{g}_I^*$ is as defined by

$$\mathbf{g}_I^* = (0, g^*, 0)^T . \tag{12}$$

T is the engine thrust which acts in the direction of the body axis and through the aircraft CG. An offset from the CG could be applied by adding an additional term to the pitching moment (thrust induced pitching moment). Expanding (6) yields the following equations for the aircraft acceleration in body axes ($\dot{w}_B^*$=0)

$$\dot{u}_B^* = \dot{\theta}^* v_B^* + g^* \sin\theta + \frac{F_x^* + T^*}{M^*} \tag{13}$$

and

$$\dot{v}_B^* = -\dot{\theta}^* u_B^* + g^* \cos\theta + \frac{F_y^*}{M^*} \tag{14}$$

Non-dimensionalising equations (13) and (14) yields

$$\dot{u}_B = \dot{\theta} v_B + g \sin\theta + \frac{\rho_\infty^* {c_r^*}^3}{M^*} \left(C_{F_x} + T\right) \tag{15}$$

and

$$\dot{v}_B = -\dot{\theta} u_B + g \cos\theta + \frac{\rho_\infty^* {c_r^*}^3}{M^*} C_{F_y} \tag{16}$$

where g is defined as

$$g = \frac{g^* c_r^*}{{U_\infty^*}^2} \tag{17}$$

Equations (15) and (16) give the aircraft accelerations in body axes. In order to take into account the translational acceleration of the aircraft, the freestream velocity vector $\mathbf{U}_I$ remains constant and the grid is moved relative to the freestream velocity. After integration of equations (15) and (16), to perform the mesh movement the velocities must be defined in the inertial (or freestream) frame of reference. This is obtained via the transformation

$$\mathbf{U}_I = \mathbf{B}^{-1} \mathbf{U}_B \tag{18}$$

Integrating equation (18) yields updated centre of gravity (CG) locations. It should be noted that the longitudinal 3 DOF equations are loosely coupled, in that they are solved sequentially (u-equation, then v-equation, then $\dot{\theta}$ equation) for each pseudo timestep. With the new CG locations and pitch attitude, the grid is rigidly translated and rotated accordingly, and the grid speeds (which simulate the acceleration of the aircraft) are computed using second order finite differences. The integration procedure is as described for the 1-degree of freedom model.

IV. Controlling the free-to-pitch motion

A. Mesh Treatment

The control decisions are felt by the aerodynamic simulation through deflections of the control surfaces. This presents the problem of first specifying the deformed aircraft shape and secondly passing this deformation to the volume grid. The volume grid also needs to be moved according to the rigid body motion (in pitch in this case) of the aircraft.

The second issue is dealt with through the method described in reference[6] which uses transfinite interpolation (TFI) to distribute applied surface grid deflections to the interior volume grid. Denote the volume grid locations as $\mathbf{x}$ and the surface grid locations as $\mathbf{x}_s$, prefix these with δ to indicate the change from the initial values and use a subscript 0 to indicate initial values, b to denote a frame of reference fixed to the aircraft and i to indicate the inertial frame used for the CFD calculations. Blending functions are used to give a relationship resulting from TFI for the volume grid deflections of the form

$$\delta\mathbf{x}_b = \mathcal{T}(\delta\mathbf{x}_{s,b}). \tag{19}$$

The new grid locations are then written as

$$\mathbf{x}_b = \mathbf{x}_{0,b} + \delta\mathbf{x}_b. \tag{20}$$

The grid locations in the interial frame are then obtained by applying rotation matrices which in the current case, for motion in pitch only, leads to

$$\mathbf{x}_i = \mathcal{P}\mathbf{x}_b \tag{21}$$

where

$$\mathcal{P} = \begin{bmatrix} cos\Theta & -sin\Theta & 0 \\ sin\Theta & cos\Theta & 0 \\ 0 & 0 & 1 \end{bmatrix}. \tag{22}$$

$$\tag{23}$$

The remaining problem is to specify the surface grid deformations $\delta\mathbf{x}_{s,b}$. There are several considerations for the choice of method. First, the geometry of the aircraft must be respected which means that an accurate surface definition, preferably from a CAD model, should be used when defining the surface grid. Secondly, since we are using deforming multiblock grids, the topology must remain fixed if regeneration of the topology itself, with an associated interpolation between grids of the CFD solution, is to be avoided. This means that part span control surfaces, not used here, are blended into the wing at their ends. Thirdly, the surface grid must be easily available over the range of possible control surfaces in an easy and computationally inexpensive manner.

These considerations have motivated the use of mode shapes to specify control surface deflections.[7] The basic idea is as follows. A mode shape is specified for each control surface separately. A surface grid is generated at the extreme deflection of the control surface, with the CAD model of the aircraft being used to specify the new geometry. Since the block topology is fixed this is a straighforward task once the initial (undeformed) CFD grid is generated. For example, using the ICEM CFD grid generator the appropriate block faces need to be reprojected onto the new CAD description. Modifying the CAD model is also reasonably straightforward since typical control surface motions involve rotations of existing components. Denote the surface grid on the geometry with the deployed control surface as $\mathbf{x}_{s,b}^{deployed}$. The process is illustrated in figure 1 for a generic aircraft test case with an all moving elevator. First, the elevator is rotated to the maximum angle ψ_{max} (in this case 10 degrees) in the CAD model and then the surface grid is reprojected onto this new CAD model. The mode shape then represents the difference between the deflected and initial surface grids, $\phi = \mathbf{x}_{s,b}^{deployed} - \mathbf{x}_{s,b,0}$.

The surface grid deflections at an intermediate control surface angle ψ_c is now approximated by scaling the mode shapes by the value ψ_c/ψ_{max}, i.e. $\delta\mathbf{x}_{s,b} = (\psi_c/\psi_{max})\phi$. This approach allows good surface grid quality to be retained, at least if control surface deflections are restricted between the extremes used to generate the surface grids which define the mode shape, and generates the required surface grids at the cost of generating a modified surface grid in the grid generation package.

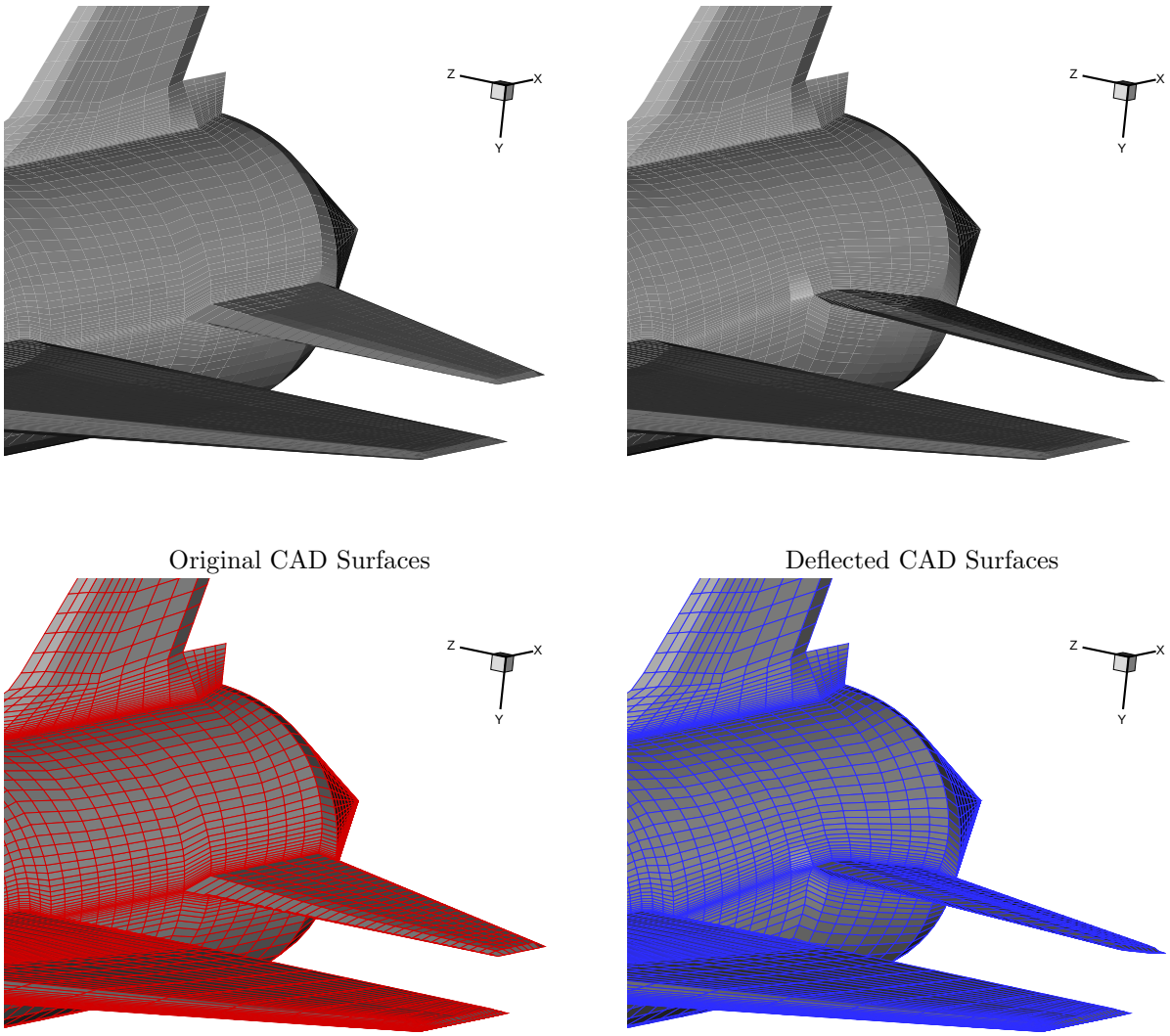

Figure 1. ***Generation of Control Surface Mode Shapes.***

Problems with this approach might arise if a control input goes outside the range used to define the mode shape, or if too large a deflection is used to define the mode shape. These cases can be catered for by using multiple mode shapes to define the influence of one control surface and summing their influence.

Finally, once the volume grid has been regenerated grid speeds are calculated using second order finite differences. It is however possible to calculate the grid speeds analytically by adding in the contributions from the TFI and the rigid rotations. This has been left to future work.

B. Trimming algorithm

The trimming algorithm described in the following sections is designed to make use of the aerodynamic updates from the dual time-stepping scheme employed in the flow solver. Standard control methods usually make use of non-linear tabular data from wind tunnel/flight tests. Here, by taking advantage of the aerodynamic updates, no *a priori* knowledge of aerodynamics is required by the trimmer. The trimmer operates within a feedback loop within the dual time-stepping scheme, where updated elevator deflections and pitching moments are fed back to the trimmer to estimate new elevator deflections.

1. Manoeuvres

In order to perform a manoeuvre to change the orientation of the aircraft (for a climb manoeuvre as an example), a desired change in orientation $\Delta\theta$ can be entered as an input to the trimmer. Thus the orientation of the fuselage relative to the inertial frame of reference can be altered. A generic variation in pitch attitude is given by

$$\theta(\tau) = \theta_0 + \frac{\Delta\theta}{2}\left(1 - \cos\frac{\pi\tau}{T}\right) \tag{24}$$

Manoeuvring the aircraft in this way prevents overshoots and allows the aircraft to manoeuvre effectively. Differentiating equation (24) yields a sinusoidal variation in pitch rate, thus midway through the manoeuvre the pitch rate is at its highest, decreasing as the desired orientation is approached. Given the desired change in pitch attitude ($\Delta\theta$), as well as the period over which the change should occur (T), the desired pitch rate of the wing ($\dot{\theta}_{reqd}$) is given by

$$\dot{\theta}_{reqd} = \frac{\pi\Delta\theta}{2T}\sin\left(\frac{\pi\tau}{T}\right) \tag{25}$$

To estimate the elevator angle required to perform such a manoeuvre, we first calculate the pitching moment that will be required to perform the manoeuvre. We can explicitly calculate this pitching moment by rearranging the integration scheme given by equation (3). Rearranging gives the explicit equation

$$C_{M_z} = \frac{J^*_{zz}}{\rho^*_\infty {c^*_r}^5}\left(\frac{2}{\Delta\tau}(\dot{\theta}_{reqd} - \dot{\theta}^n) - \frac{\rho^*_\infty {c^*_r}^5}{J^*_{zz}} C^n_{M_z}\right). \tag{26}$$

Entering the desired pitch rate $\dot{\theta}_{reqd}$ into equation (26), we get the pitching moment required to perform the manoeuvre. Although a sinusoidal variation in pitch rate is assumed, any pitch rate history can be applied. In equation (26) C_{M_z} is the pitching moment required to accelerate the aircraft, $C^n_{M_z}$ is the pitching moment from the previous time step, $\dot{\theta}_{reqd}$ is the required pitch rate calculated from the aircraft deceleration rate, and $\dot{\theta}^n$ is the pitch rate from the previous time step.

Given the pitching moment required to perform a desired manoeuvre we must now estimate the elevator deflection which will give the required pitching moment. This is done iteratively. At the start of each time step, the elevator is perturbed a small amount which starts the method. Based on the results of this perturbation a new elevator angle is estimated by assuming the gradient $\frac{\partial C_{M_z}}{\partial \delta_E}$ to be equal to that obtained from the previous iteration. This yields the iteration scheme

$$\frac{C^{n+1,k}_{M_z} - C^n_{M_z}}{\delta^{n+1,k}_E - \delta^n_E} = \frac{C^{n+1,k+1}_{M_z} - C^{n+1,k}_{M_z}}{\delta^{n+1,k+1}_E - \delta^{n+1,k}_E}. \tag{27}$$

During a time step we are trying to drive the pitching moment to the required value, and so in equation (27) we replace $C^{n+1,k+1}_{M_z}$ with the required pitching moment C_{M_z}, and solve for $\delta^{n+1,k+1}_E$. This iteration procedure continues throughout the time step. In equation (27) $\delta^{n+1,k+1}_E$ is the updated elevator deflection,

$\delta_E^{n+1,k}$ is the elevator deflection from the previous pseudo iteration, δ_E^n is the elevator deflection from the previous timestep, $C_{M_z}^{n+1,k}$ is the pitching moment from the previous pseudo iteration, and $C_{M_z}^n$ is the pitching moment from the previous timestep. The convergence depends on the accuracy of the updated pitching moment $C_{M_z}^{n+1,k}$, which is taken as the pitching moment associated with the elevator deflection $\delta_E^{n+1,k}$. To provide accurate updates for the pitching moment associated with an elevator deflection $\delta_E^{n+1,k}$, the elevator position is only updated every second pseudo iteration, allowing sufficient convergence of $C_{M_z}^{n+1,k}$ to provide an accurate elevator deflection at the end of the time step. It should be noted that the elevator deflection is constrained by a user specified maximum elevator rate. Since the aerodynamic derivative $\frac{\partial C_{M_z}}{\partial \delta_E}$ is expected to vary linearly over one time step, the described method should converge well.

Example convergence histories of the pitching moment and elevator deflection are given for a case limited by the elevator deflection rate (figure 2), and for a case where the elevator reaches its desired location (figure 3) within the time step. In the limited case the required pitching moment cannot be reached within one time step. As such the elevator angle is limited to its maximum deflection for that time step. In the unlimited case the method described converges well.

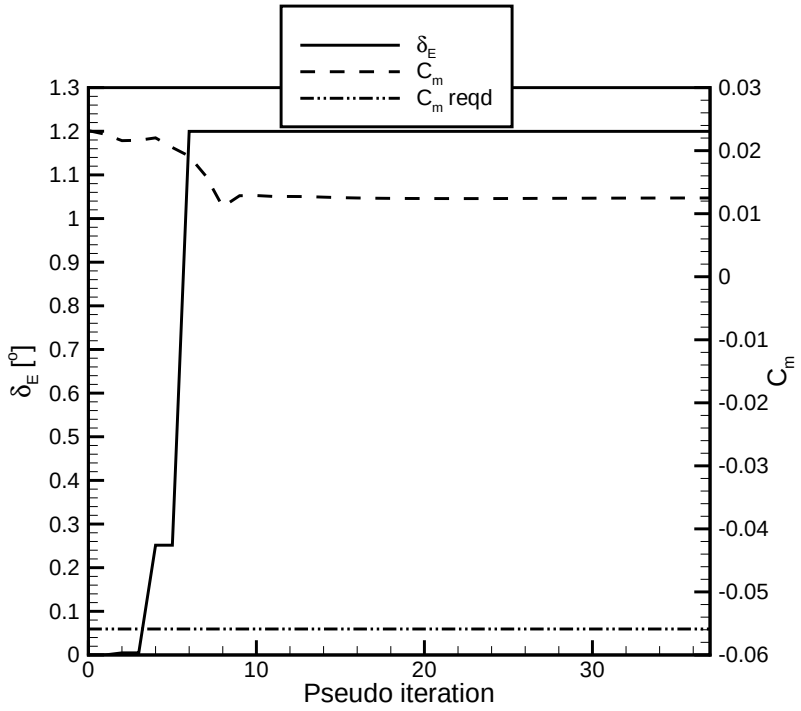

Figure 2. ***Convergence of elevator angle and pitching moment coefficient for one time step - Limited by*** δ_E

2. Hold angle of attack

Either before or after a manoeuvre we may wish to hold the current angle of attack. For a given flight condition (elevators fixed), as the simulation proceeds the aircraft will either pitch up or down based on the pitching moment around the centre of gravity (which is dependent of the angle of attack of the aircraft and the elevator incidence relative to the fuselage axis). If the aircraft is pitching we wish to set the pitch rate to zero. When the trimmer is turned on the algorithm begins by estimating the elevator deflection required to bring the pitch rate to zero. This requires a non-zero pitching moment in the opposite sense to the moment driving the pitching motion. When eventually both the pitch rate and moment are zero, the aircraft is trimmed.

Realistically we do not wish to bring the aircraft from its current pitch rate to zero within one trim step, therefore we must define an aircraft acceleration, $\ddot{\theta}_{ac}$ to constrain the motion. We therefore calculate the pitch rate desired at the end of the time step within the constraint of the acceleration rate of the aircraft.

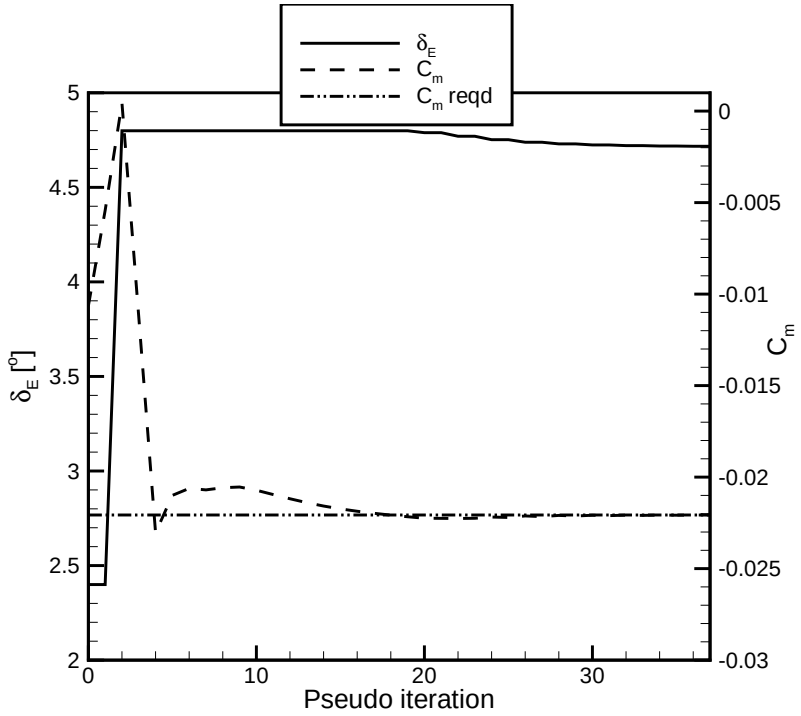

Figure 3. ***Convergence of elevator angle and pitching moment coefficient for one time step***

The pitch rate at the end of the time step is calculated using

$$\dot{\theta}_{reqd} = \dot{\theta}^n - Sign(\dot{\theta}^n)\ddot{\theta}_{ac}\Delta\tau \tag{28}$$

Using the pitch acceleration $\ddot{\theta}_{ac}$ as a limiter, we calculate the pitching moment needed to give the required pitch rate $\dot{\theta}_{reqd}$ using equation (26). From equation (26) it can be seen that the pitching moment required to accelerate the aircraft is simply a restoring moment to counter the current pitching moment, as well as an additional amount required to counter the angular momentum. In a similar manner to the manoeuvring case we require to estimate the elevator deflection to give the required pitching moment. Again this is done iteratively as in equation (27). However, rather than linearising from the previous timestep we linearise from the point when the trimmer is turned on to prevent divisions by zero (as would be the case if we used the iteration scheme given by equation (27)). The iteration scheme employed is given by

$$\frac{C_{M_z}^{n+1,k} - C_{M_z}^{0}}{\delta_E^{n+1,k} - \delta_E^{0}} = \frac{C_{M_z}^{n+1,k+1} - C_{M_z}^{n+1,k}}{\delta_E^{n+1,k+1} - \delta_E^{n+1,k}}. \tag{29}$$

where δ_E^0 and $C_{M_z}^0$ are the elevator deflection and pitching moment at the beginning of the trimming procedure.

V. Test cases

The test case for the current simulations is the Standard Dynamics Model (SDM).[5] The SDM has been used in the investigation of wing and fin buffet associated with vortex breakdown at high incidence.[5] The model is a generic fighter aircraft configuration (based on the F-16) which consists of a cylindrical fuselage section, a leading edge extension (for the generation of vortical flow), wings with sharp leading edges, elevators (all moving in the current simulations), a vertical fin, canopy, and a cone section at the rear of the fuselage. The cone replaces the sting which was present in experiments and is necessary as we are conducting Euler simulations and no jet condition is applied. Given the similarity of the model to the F-16, the inertial data for an F-16[4] was used. The centre of gravity was located at $2.2c_r$ from the nose of the aircraft to make

the configuration unstable for the one degree of freedom calculations. Clearly changing the centre of gravity location will change the moments of inertia of the aircraft. However in the current work only indicative inertia values are required. Table 1 shows the initial test conditions used in all the described simulations.

Mach number	0.8
Angle of attack	3^o
ρ_∞	$1.23kgm^{-3}$
c_r	3.45m
x_{cg}	$2.25c_r$
J_{zz}	$75651Nm^2$
Aircraft pitch acceleration	$45^o s^{-2}$
Max elevator pitch rate	$60^o s^{-1}$

Table 1. Flow conditions

Since we are dealing with longitudinal motion, only half of the aircraft was modelled with a symmetry condition applied at the centreplane. The grid which is of an "O" topology around the streamwise direction, consists of 32 blocks with approximately 410,000 grid points.

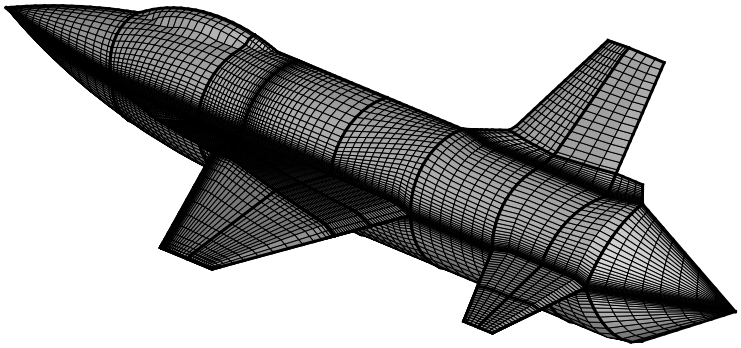

Figure 4. ***Surface mesh***

VI. One degree of Freedom Results

A. Steady state calculation

Before commencing simulations of the free response of the SDM, a steady state calculation was performed. The flow conditions (as specified in table 1) were a freestream Mach number of 0.8 and an incidence of 3^o. The elevators were fixed in position at 0^o relative to the fuselage axis. The lift coefficient obtained was 0.084, which after re-dimensionalising and assuming steady level flight, yields a lift force balancing an aircraft mass

of approximately 9100Kg (the mass of the F-16 is approximately 9300Kg[4]). With the elevators fixed at 0^o there is a slight nose-up pitching moment making the configuration unstable (C_{m_α} is positive).

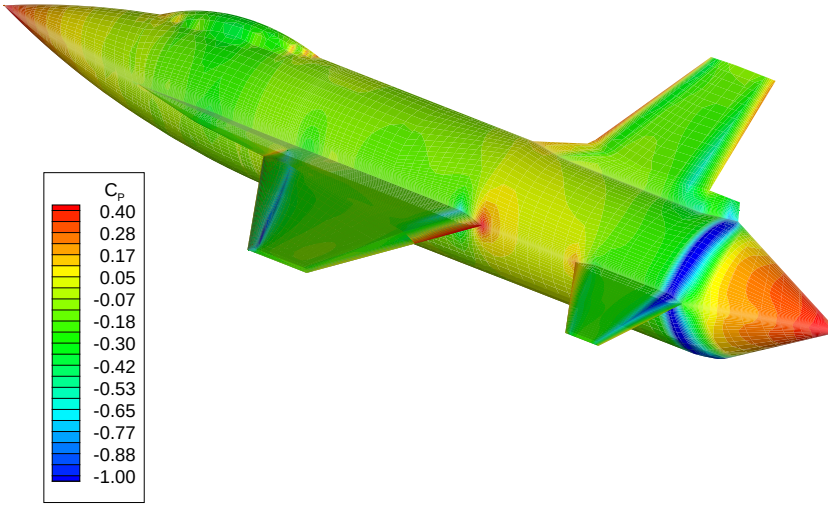

Figure 5. ***Surface pressure distribution over SDM at*** 3^o ***incidence and M=0.8***

The surface pressure distribution over the model is shown in figure 5. Since the Euler equations are solved the flow acceleration over sharp changes in geometry (near the leading edge of the wing and at the beginning of the cone at the end of the fuselage) can be seen as dark blue regions. With the grid density used and the low incidence, there is little or no indication of a vortex forming at the leading edge extension.

B. Free-to-pitch simulation - No control

Before applying any form of control to the model, a free-to-pitch simulation was performed. The initial conditions were 2^o angle of attack at zero pitch rate, with the elevators fixed at 0^o relative to the fuselage axis. As previously mentioned with this elevator setting the model is unstable with a nose up pitching moment. Figure 6 shows the angle of attack and pitch rate histories, and figure 7 shows the lift and pitching moment coefficient histories. Clearly with no control the aircraft pitches up under the influence of the nose-up pitching moment, with the pitch rate increasing as the pitching moment increases (with incidence). As the incidence increases the lift coefficient also increases, reaching a maximum around τ=75.

C. Free-to-pitch simulation - Hold incidence

Given the results of the simulation for the free-to-pitch motion without control, a simulation was conducted to immediately trim the aircraft and hold the angle of attack. The initial angle of attack of the aircraft is 4^o and the initial elevator setting is 0^o relative to the fuselage axis. After one time step (to allow the aircraft pitch rate to become non-zero) the trimmer was turned on. As described earlier the trimmer is limited by the pitch rate of the elevator, and as such time is required for the elevator to bring the aircraft pitch rate to zero. This is due to the fact that the initial elevator setting of 0^o is relatively far from the elevator setting required to trim the aircraft. Examination of the trim histories during the initial time steps showed convergence histories (during the pseudo iterations for a physical time step) of C_m and δ_E similar to those shown in figure 2. In other words at the beginning of the trimming procedure, the time taken for the elevator to reach its required position prevents the aircraft trimming immediately, and as such the incidence

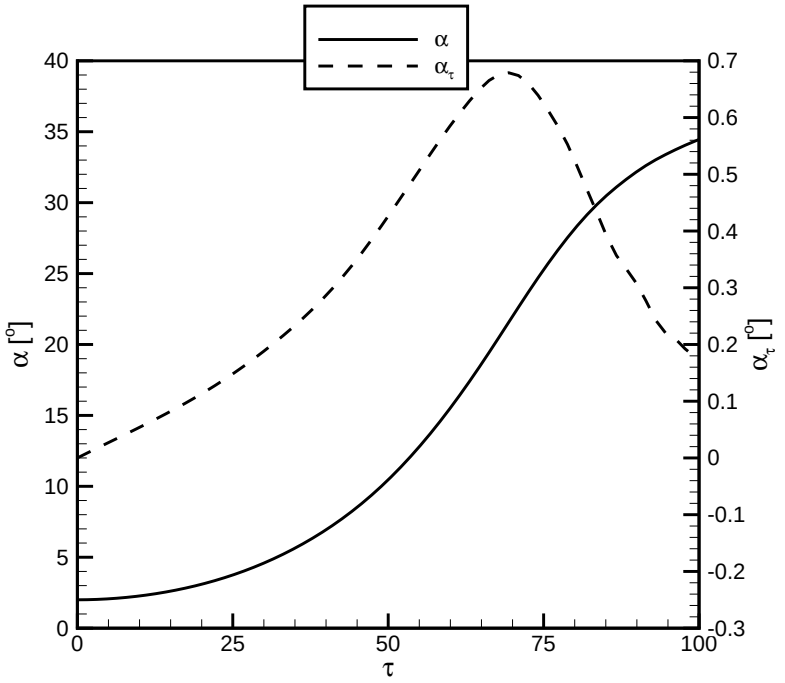

Figure 6. *Free to pitch motion without control - Angle of attack and pitch rate histories*

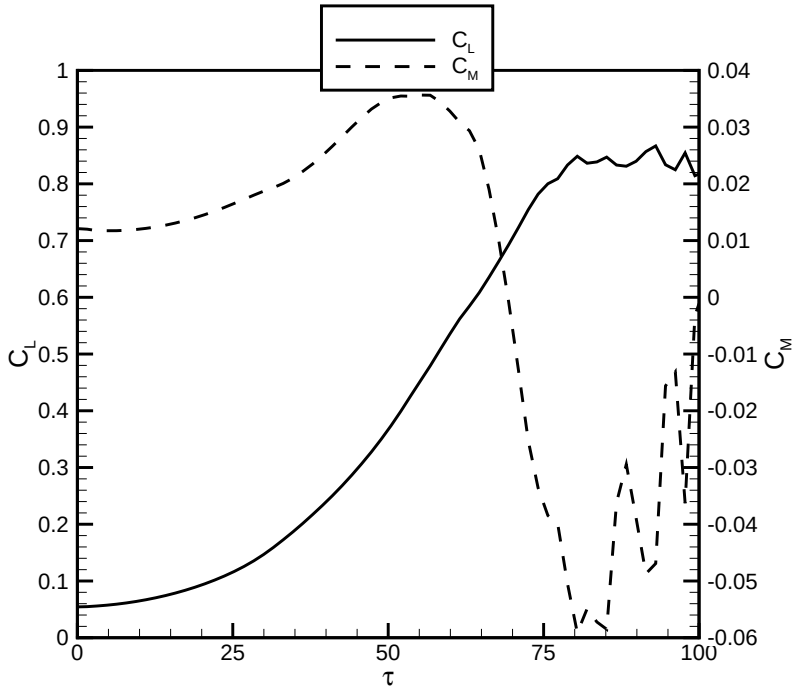

Figure 7. *Free to pitch motion without control - Lift and pitching moment coefficient histories*

of the aircraft increases slightly under the influence of the initial nose up pitching moment. Eventually the elevator is able to reach the required settings and the trim histories resemble those shown in figure 3.

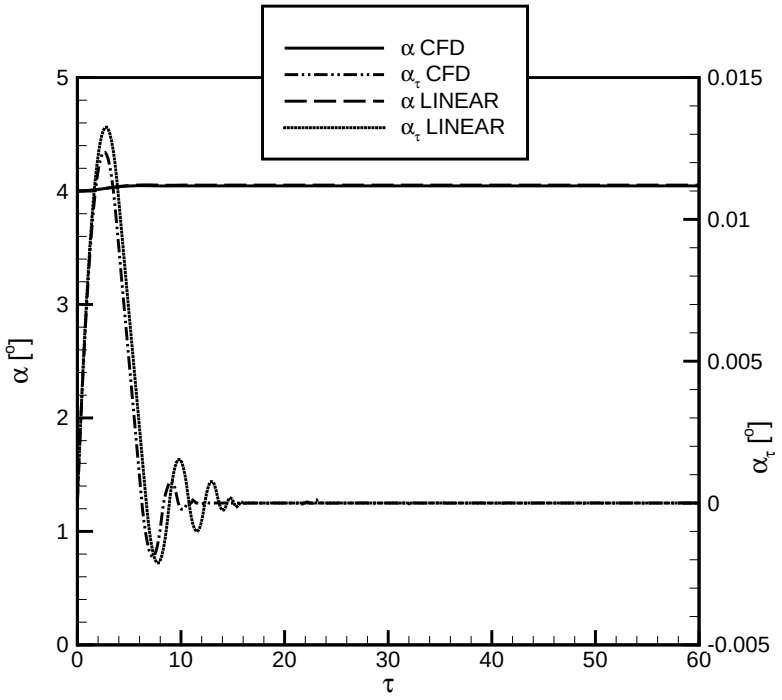

Figure 8. ***Free to pitch motion with trimmer holding angle of attack - Angle of attack and pitch rate histories***

The angle of attack and pitch rate histories for the hold incidence case are shown in figure 8, where results from simulations using a full time accurate CFD model and a linear model of the aerodynamics,[4] are shown. The pitching moment and lift coefficient histories are shown in figure 9 (where only results from the full CFD model are shown), and the elevator deflection histories are shown in figure 10 (for both the full CFD and linear models). As previously discussed, it can be seen in figure 8 that the aircraft angle of attack increases slightly while the trimmer brings the aircraft under control. If we examine the pitch rate histories from the full CFD model, it is clear that the positive pitch rate initially increases due to the nose up pitching moment whilst the elevator moves in to place. As the elevator gets close to the trim position the positive pitch rate decreases, becoming negative at around $\tau = 6$. As the trimmer continues to adjust the pitch rate becomes positive again, with the oscillations quickly damping out leaving a zero pitch rate for all $\tau > 12$.

Examining the lift and pitching moment coefficients in figure 9 it is clear that despite the aircraft pitch rate being near zero, there are still minor adjustments being made by the trimmer (though it is clear that the amplitude of these adjustments decreases with time). However this may be expected given that the aircraft is unstable and any small perturbations will grow with time unless the trimmer acts upon them.

It is clear from the elevator deflection histories in figure 10, that as the trimmer is turned on and the aircraft begins to pitch up, the trimmer applies an increasing angle of attack of the elevator to counter the nose up moment and pitch rate. The linear variation in elevator angle with time during the period $0 \leq \tau \leq 4$, is due to the elevator pitching at its maximum rate to reach the required trim position as quickly as possible. It should be noted that the rate at which the elevator pitches up is equal to its maximum allowable pitch rate of 60^o/s. It can be seen in figure 9 that as increasing elevator is applied, the pitching moment quickly reduces and begins to decelerate the aircraft pitch rate at around $\tau = 3$. Similary as the pitch rate begins to slow the elevator angle is reduced until approximately $\tau = 9$. Comparing the elevator histories from both the full CFD and linear models, it can be seen that the elevator deflections are of a lower magnitude in the full CFD simulations in comparison to the linear model solutions. This reduces the damping in the linear model solutions and may be due to the inaccuracy of using constant stability derivatives in the linear model.

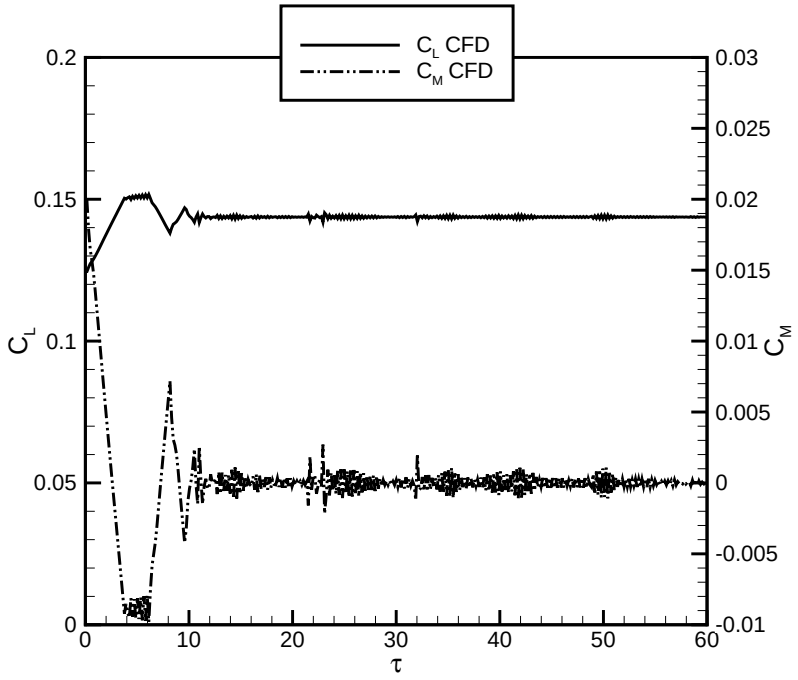

Figure 9. *Free to pitch motion with trimmer holding angle of attack - Lift and pitching moment coefficient histories*

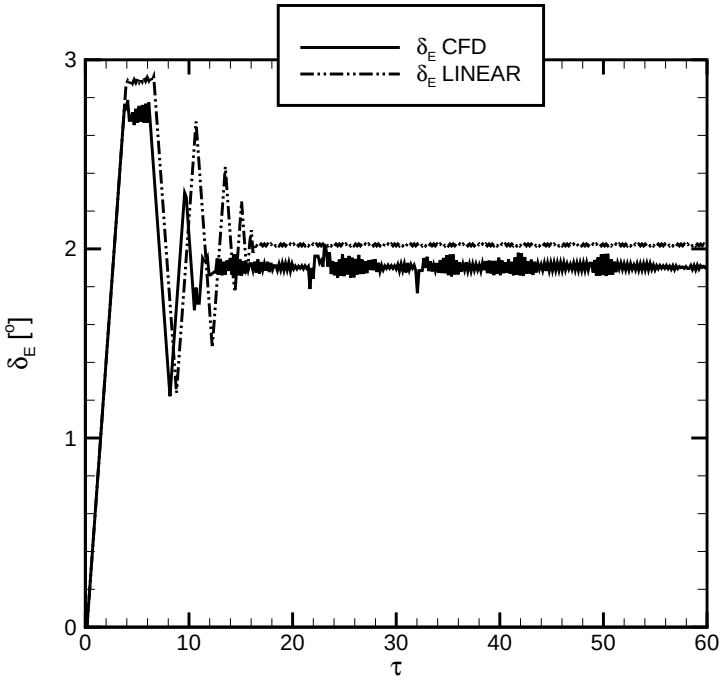

Figure 10. *Free to pitch motion with trimmer holding angle of attack - Elevator deflection histories*

D. Free-to-pitch simulation - Prescribed manoeuvre

Given that with control surface deflections we can hold the angle of attack of the aircraft, we now perform a simulation of a specified manoeuvre. In this case we initially want to hold the angle of attack as in the case of section C. However, once the aircraft is trimmed we wish to increase the angle of attack by 7^o in a time of $\tau = 250$. As described earlier, a sinusoidal variation in pitch rate is assumed throughout the duration of the manoeuvre. This prevents overshoots in the angle of attack.

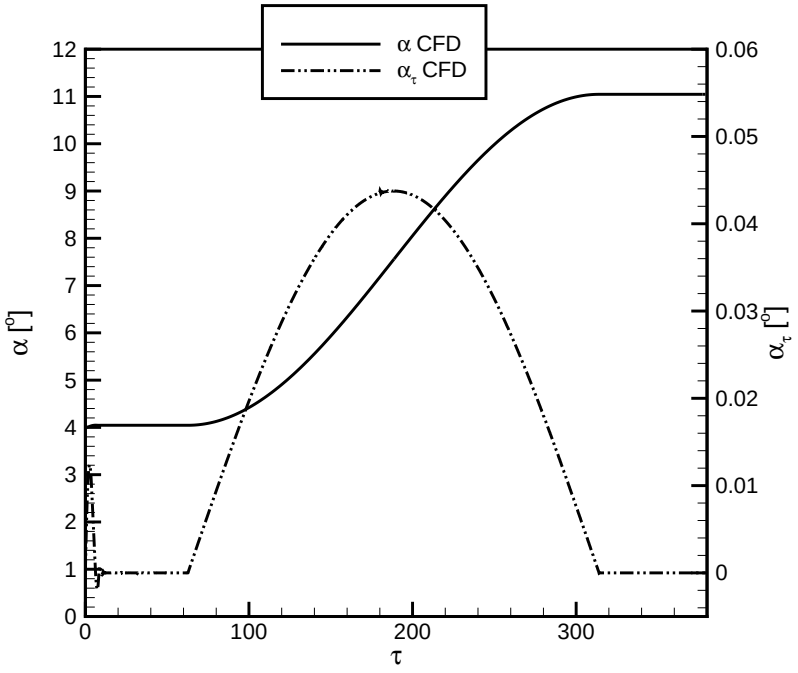

Figure 11. *Free to pitch motion with trimmer manoeuvring aircraft - Angle of attack and pitch rate histories*

The angle of attack and pitch rate histories for the manoeuvring case are shown in figure 11 (where only results from the full CFD model are shown). It should be noted that this simulation was also conducted using the linear model and that the pitch angle and rate curves lie on top of the curves presented in figure 11. The pitching moment and lift coefficient histories are shown in figure 12 for the full CFD model, and the elevator deflection histories from both the full CFD and linear models are shown in figure 13. Considering first the pitch angle and rate histories, it is clear that the commanded sinusoidal variation in pitch rate is obtained, and that the aircraft incidence has increased by 7^o as requested. The aircraft initially trims well at 4^o angle of attack, and after a time of $\tau = 60$, the aircraft performs a pitch up manoeuvre to increase the incidence by 7^o.

As in the case where the aircraft is held at a constant angle of attack, there are slight fluctuations in the pitching moment and lift coefficient curves throughout the hold, manoeuvre, and final hold (see figure 12). Again this is due to an oscillation in the elevator motion as seen in figure 13. During the hold incidence portions of the load and moment histories there are decaying oscillations as in section C, with slightly larger oscillations in pitching moment during the duration of the manoeuvre. This is due to the fact that the trimmer is forcing the unstable aircraft to follow the commanded sinusoidal variation in pitch rate, thus the elevator has to constantly make corrections.

Finally we compare the elevator histories from the full CFD and linear models given in figure 13. Both the full CFD and linear models exhibit minor fluctuations in elevator angle throughout the histories. Clearly there is a discrepancy between the full CFD model and linear solutions with respect to the elevator histories. As previously discussed this is most likely due to errors associated with the constant coefficient linear model.

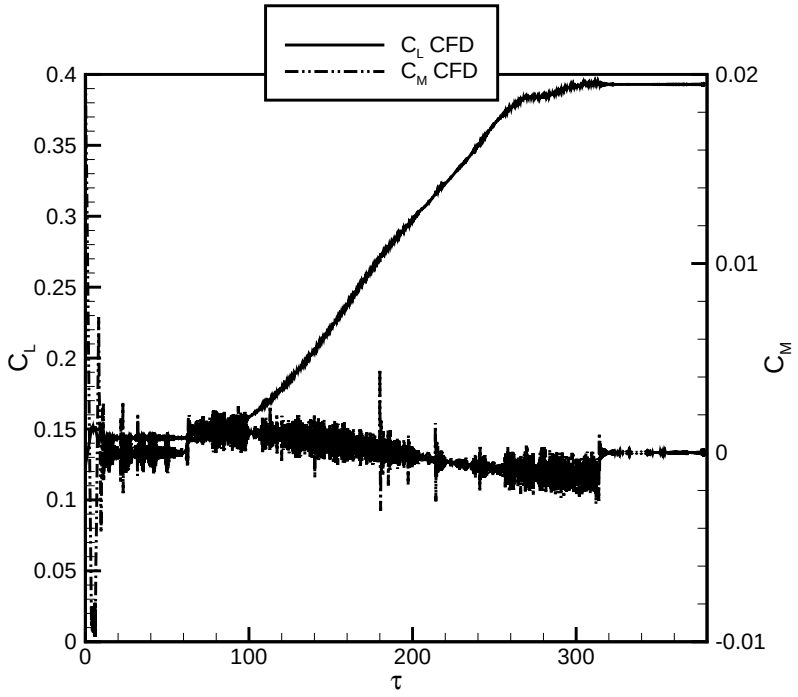

Figure 12. *Free to pitch motion with trimmer manoeuvring aircraft - Lift and pitching moment coefficient histories*

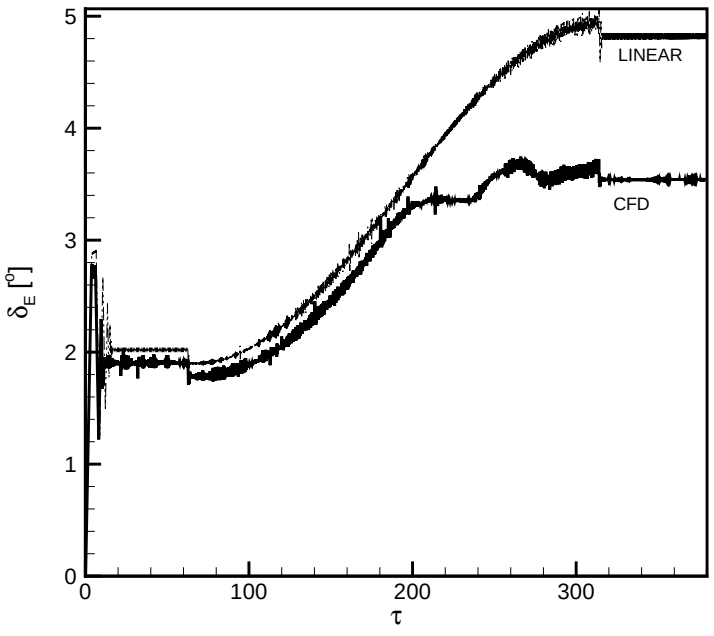

Figure 13. *Free to pitch motion with trimmer manoeuvring aircraft - Elevator deflection histories*

Mach number	0.5
Angle of attack	3^o
Elevator angle	-1.93^o
Aircraft Mass	3143Kg
Root chord	3.45m
J_{zz}	$75651Kg - m^2$
Air density	$1.23\frac{Kg}{m^3}$

Table 2. Trim conditions

E. Three degree of Freedom Results

An additional test case was the controlled longitudinal 3 DOF flight of the SDM geometry. In order to trim the aircraft, the trimmer was applied to eliminate pitch rates as previously described. To trim the aircraft in the translational sense, a low engine thrust was applied (acting through the cg) with the mass of the aircraft being set such that no translational accelerations were present. The trim conditions obtained are as follows

Recall that the wing and tail of the SDM have a flat upper and lower surface, therefore the lift predicted is low. Also the Euler equations are used thus the drag is small (theoretically the drag would be zero in the absence of numerical effects). Figure 14 shows the angle of attack and pitch angle histories of the SDM after an elevator doublet of $\pm 2^o$. Also shown is the response of the F-16 to the same doublet elevator input for comparison purposes. It should be stressed that the F-16 result is given to compare trends only, since differences in parameters such as cg location, lift curve slope etc., will effect the response and damping (of both the short period and phugoid modes) of the motion. As the aircraft pitches down under the influence of the positive elevator deflection, the lift of the aircraft decreases and the aircraft decends. This results in a change in the angle of attack of the aircraft (as well as pitch angle), which due to the additional downward velocity component is less than the change in pitch angle (θ). As the elevator is deflected in the opposite sense, the aircraft nose lifts up and lift is restored, increasing as angle of attack increases. Again due to the fact that as the SDM increases angle of attack and lift becomes greater than weight, the aircraft climbs, increasing the angle of attack further than the pitch angle, due to the additional velocity components associated with climbing flight. As the elevator is set back to the trim condition the aircraft reponds with a damped short period and phugoid mode as it settles back to the trim condition. From figure 14 it is clear that the short period mode of the SDM is slightly less damped than the F-16, as is the phugoid mode which is apparent in the gradual change in θ which will oscillate eventually becoming zero at some later time. However, it is clear that the coupled CFD / 3 DOF model performs well.

VII. Conclusions

The calculation of trimmed longitudinal flight of an unstable generic fighter configuration has been demonstrated, using coupling between CFD and one and three degree-of-freedom equations. A simple controller has been implemented to allow a prescribed motion to be followed (including trimmed flight). Whilst the flight mechanics and control are relatively simple the demonstration has achieved the following

- the various grid motions necessary (including applied elevator motions and rigid body rotations) have been achieved in a straightforward fashion which can be generalised to more demanding cases
- the coupling between the flight mechanics and aerodynamic equations, and incorporating a controller, has been built into the pseudo time loop successfully
- the generalisation to include flexibility effects is straightforward and will allow time domain simulations for flight and aeroelastic stability
- the cost of the calculations is not prohibitive for isolated flight manoeuvres

Future work and questions are

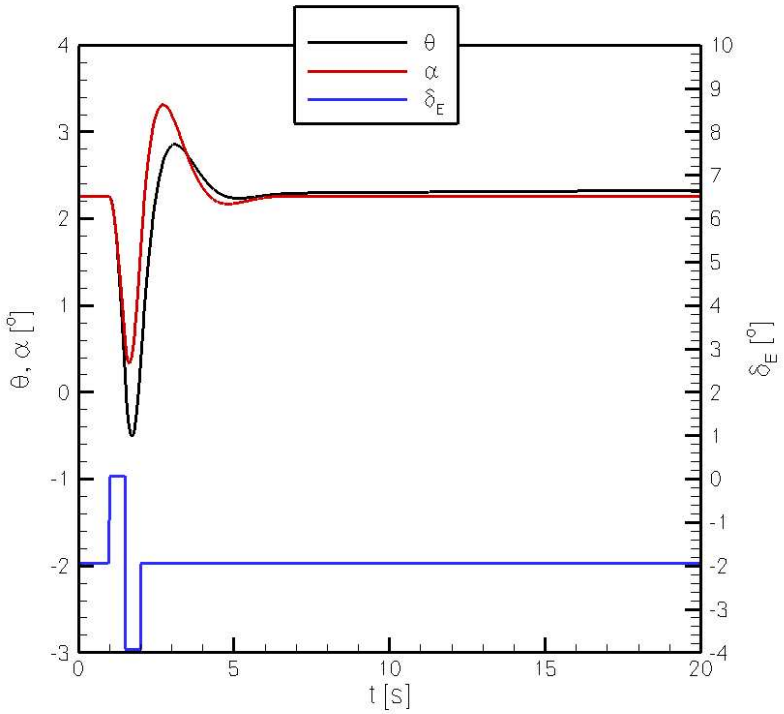

Figure 14. ***Three degree of freedom response to an elevator doublet.***

- the generation of a full derivative based flight mechanics model for evaluation of the CFD generated motions
- the simulation of motions in regions where the derivative type model is likely to be unsatisfactory, such as when vortical flows introduce hysteresis

VIII. Acknowledgements

This work forms part of the Defence and Aerospace Research Partnership in Unsteady Flow Methods (PUMA DARP) and was funded by BAE SYSTEMS, Engineering and Physical Sciences Research Council, Ministry of Defence and Department of Trade and Industry. This report is Deliverable D.1.15a of this programme.

References

[1]Jenkins, J.E., Myatt, J.H. and Hanff, E.S., Body-Axis Rolling Motion Critical States of a 65-Degree Delta Wing, Journal of Aircraft, vol 33, No 2, 1996.

[2]Badcock, K.J., Richards, B.E., and Woodgate, M.A., "Elements of Computational Fluid Dynamics on block structured grids using implicit solvers, Progress in Aerospace Sciences, Vol. 36, pp 351-392, 2000.

[3]Jameson, A., "Time dependent calculations using multigrid, with applications to unsteady flows past airfoils and wings", AIAA Paper 91-1596, 1991.

[4]Stevens, B. L., and Lewis, F. L., "Aircraft simulation and control", ISBN 0-471-61397-5, John Wiley and Sons Inc, 1992.

[5]Huang, X. Z., "Wing and fin buffet on the standard dynamics model", RTO Technical Report 26 - Verification and validation data for computational unsteady aerodynamics, October 2000.

[6]L.Dubuc, F.Cantariti, M.Woodgate, B.Gribben, K.J.Badcock, and B.E.Richards, *A grid deformation technique for unsteady flow computations*, Int J Num Meth Fluids,32 pp 285-311, 2000.

[7]Boelens, O., Private Communication.